THE JOURNAL OF PHYSICAL CHEMISTRY Letters

pubs.acs.org/JPCL Letter

Quantum Device Emulates the Dynamics of Two Coupled Oscillators

Ksenia Komarova, Hugo Gattuso, R. D. Levine, and F. Remacle*

Cite This: J. Phys. Chem. Lett. 2020, 11, 6990−6995 Read Online

ACCESS | Metrics & More | Article Recommendations | Supporting Information

ABSTRACT: Our quantum device is a solid-state array of semiconducting quantum dots that is addressed and read by 2D electronic spectroscopy. The experimental ultrafast dynamics of the device is well simulated by solving the time-dependent Schrödinger equation for a Hamiltonian that describes the lower electronically excited states of the dots and three laser pulses. The time evolution induced in the electronic states of the quantum device is used to emulate the quite different nonequilibrium vibrational dynamics of a linear triatomic molecule. We simulate the energy transfer between the two local oscillators and, in a more elaborate application, the expectation values of the quantum mechanical creation and annihilation operators of each local oscillator. The simulation uses the electronic coherences engineered in the device upon interaction with a specific sequence of ultrafast pulses. The algorithm uses the algebraic description of the dynamics of the physical problem and of the hardware.

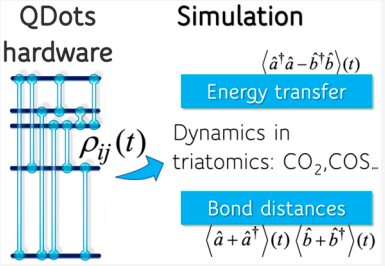

About 40 years ago in a highly cited paper,[1] Feynman reflected on simulating physics with computers. One of the two main options that Feynman discussed was using a new kind, a quantum computer, to simulate other quantum systems (section 4 of ref 1). Feynman remarked that there can be a class of intersimulatable systems and possibly there can also be a universal machine. Here we discuss the former, more limited class with a specific application.

In the intervening years, there was spectacular progress in the theory of quantum computing,[2−15] not all of which related to the vision of Feynman. An arguably concrete demonstration of quantum supremacy has been published by the Google team.[11] Quantum computing algorithms also start to be applied to simulate quantum many-body problems in physics and chemistry,[12−15] with special reference to eigensolvers.[16−18] Quantum-enhanced machine learning algorithms[19] that take advantage of the new capabilities of quantum computers for linear algebra operations are being actively developed.[14,20,21] Such algorithms include principal component analysis canonical correlation analysis and other algebraic methods used for dimension reduction. Quantum algorithms are also being developed for sampling probability distributions.[22] The debate remains open at to which physical hardware support is most suitable for quantum computing[23] and what will be the optimal quantum architecture, standalone computer, or task-dedicated module integrated into hybrid quantum classical architecture.[24] Here we go back to the classification of Feynman and describe a class of intersimulatable machines in which a member of the class has been realized experimentally on a solid-state array of CdSe QDs.[25,26] The special point about the class is that we describe dynamics, not only energetics.

The hardware we consider is an array of semiconducting quantum dots, QDs. Each dot has lower-lying electronically excited states with absorption in the visible within the coherence bandwidth of a fast laser. Addressing the device by a sequence of laser pulses and read-out is performed simultaneously on many dots[25−30] as in 2D electronic spectroscopy.[31,32] Reading many dots concurrently means that each value is read many times so that the observed mean value is the true average, similarly to NMR quantum computing.[33] Measuring over a classical ensemble of dots importantly means that there is practically no interference between measuring different observables that individually do not commute and so are not subject to a quantum uncertainty principle. There is, however, a negative side: the size variability of quantum dots means that the different dots are not quite identical and one must average the read-out over the distribution of sizes. This limits the frequency resolution or, equivalently, the time available for read-out[34] to faster than the coupling to phonons and in that time scale for the device operates on a purely electronic spectrum of an isolated system. We theoretically describe the device as an N-state quantum system. At the moment, it is the finite size dispersion of the dots as synthesized in the better experiments, say 5% or below, that limits the frequency resolution of the read-out by limiting the number of distinct states that can be resolved.

The physics of an N-state quantum system, $|i\rangle$, $i = 1, 2,.., N$, is fully described by N^2 real variables that we chose as the N occupation probabilities, $N - 1$ if we impose normalization and $N(N - 1)$ real valued coherences. We think of these numbers as expectation values of N^2 Hermitian operators, one

Received: June 17, 2020
Accepted: August 4, 2020
Published: August 4, 2020

https://dx.doi.org/10.1021/acs.jpclett.0c01880
J. Phys. Chem. Lett. 2020, 11, 6990−6995

of which is the identity operator, $\hat{I}$. A carat superscript will be used to denote an operator. The N^2 operators induce transitions between quantum states, and their expectation values are the logic variables. The operators are our analogues of the logic gates of quantum computing. It is sometimes simpler to use non-Hermitian operators, specifically $\hat{X}_{ij} \equiv |i\rangle\langle j|$ where the Hermitian operators are $(\hat{X}_{ij} + \hat{X}_{ji}/2)$ and $(\hat{X}_{ij} - \hat{X}_{ji})/2i$. We tend to think of $\hat{X}_{ij} \equiv |i\rangle\langle j|$ as a coherence because its expectation value is the coherence between states i and j. Scheme 1 on the left shows the algebra for a system with a ground and two accessible excited levels, $i, j = 0, 1, 2$ or $N = 3$ that is a simple hardware. Quite different algebra for the two coupled oscillators we mean to emulate is shown on the right.

Scheme 1. Operators and Their Evolution in the Hardware (Single QD) and in the Physical System

Hardware algebra

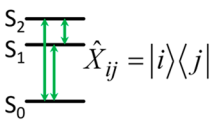

$$\hat{X}_{ij} = |i\rangle\langle j|$$

$$d\hat{X}_{ij}/dt = i\left[\hat{H}, \hat{X}_{ij}\right] = i\sum_{k,l=1}^{N} x_{ij,kl}\hat{X}_{kl}$$

Simulation algebra

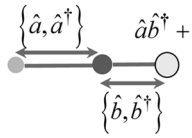

$$\frac{d}{dt}\begin{pmatrix}\hat{a}\\ \hat{a}^\dagger\\ \hat{b}\\ \hat{b}^\dagger\end{pmatrix} = \begin{pmatrix}-i\omega_a & 0 & -i\alpha/2 & 0\\ 0 & i\omega_a & 0 & i\alpha/2\\ -i\alpha/2 & 0 & -i\omega_b & 0\\ 0 & i\alpha/2 & 0 & i\omega_b\end{pmatrix}\begin{pmatrix}\hat{a}\\ \hat{a}^\dagger\\ \hat{b}\\ \hat{b}^\dagger\end{pmatrix}$$

In 2D electronic spectroscopy, the laser pulses optically connect the different states of the systems, which means[35,36] that the set of N^2 operators is closed under commutation with the Hamiltonian, $[\hat{H}, \hat{X}_{ij}] = \sum_{k,l=1}^{N} x_{ij,kl}\hat{X}_{kl}$. The rate of change of the operators and thereby the rate of change of their mean values over the ensemble are therefore closed:

$$(\mathrm{d}\langle\hat{X}_{ij}\rangle/\mathrm{d}t) = \mathrm{i}\langle[\hat{H}, \hat{X}_{ij}]\rangle = i\sum_{k,l=1}^{N} x_{ij,kl}\langle\hat{X}_{kl}\rangle \quad (1)$$

The closure property defined on the operators means that eq 1 is valid for any density matrix $\hat{\rho}$ of the isolated system, pure or mixed, $\langle\hat{X}_{ij}\rangle \equiv \mathrm{Tr}(\hat{\rho}\hat{X}_{ij})$. Equation 1 allows our physical device (i.e., the hardware) to emulate the time dependence of the N^2 values $\langle\hat{X}_{ij}\rangle$ starting from their value in the initial state and the parameters of the lasers and the transition dipoles. We have shown[25,26] that the experimental response of our hardware is well reproduced by a numerical solution of eq 1 using quantum chemical computations of energy levels and transition dipoles. We will use this numerical solution here.

All quantum systems for which we can determine up to N^2 operators that are closed under commutation with the Hamiltonian are therefore intersimulatable by a suitable arrangement of the addressing of the computing device by the laser pulses. One can exhibit the output for a particular input as a 3D map. By convention, one axis is the time interval T between the second and third laser pulses, so we show the read-out from the device as a series of 2D maps in which each one is a cut of the 3D map at a particular value of T. Closure under commutation with the Hamiltonian is relevant only during the time when the evolution is unitary, meaning the time when the system is effectively not coupled to its environment. This is only realistic for a short time, so we limit our attention to systems that can be read within that short time. A special but very common case of a system admitting an algebra of N^2 operators that are closed under commutation with the Hamiltonian is a quantum mechanical system of N states. But there are more general cases, and in the example we discuss in the main text we demonstrate the closed algebra of five and nine operators. What is needed is that the expectation values of the operators in the algebra are sufficient to specify the initial state of the system we mean to simulate.

We discuss a linear molecule (e.g., COS) with two harmonic local stretches. Of course such a system is analytically soluble, giving rise to symmetric and antisymmetric vibrational normal

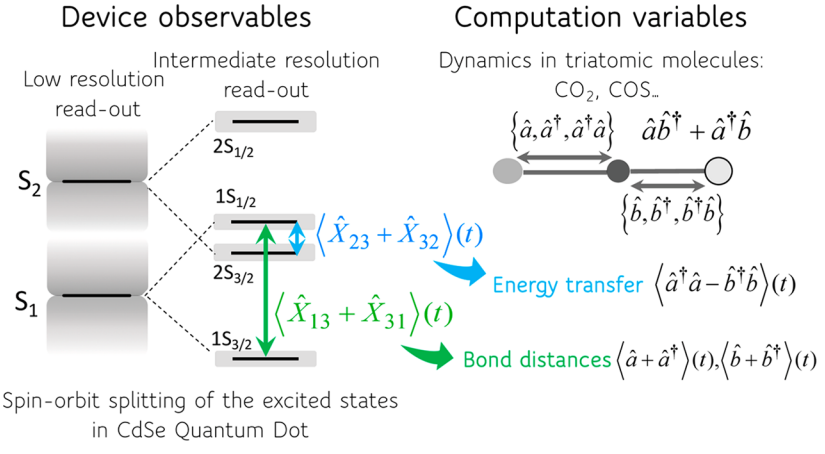

Figure 1. Realization of the concept. (Left) Two lowest excited states of a single dot. At the lowest resolution, each state is an unresolved band of 12 quantum states as mimicked by the shading. At an intermediate resolution that is achievable by experiments at room temperature, each band is split by spin−orbit coupling into two bands of four and eight states, respectively. See Figures S2 and S3 of the SI for more details. (Right) Coupled oscillator system and two time-dependent mean values, energy transfer, and bond oscillation, which can be simulated. Intermediate resolution allows resolving up to 5^2 variables. The same number of variables can be simulated using a QD dimer read at the lowest spectroscopic resolution.

https://dx.doi.org/10.1021/acs.jpclett.0c01880
J. Phys. Chem. Lett. 2020, 11, 6990−6995

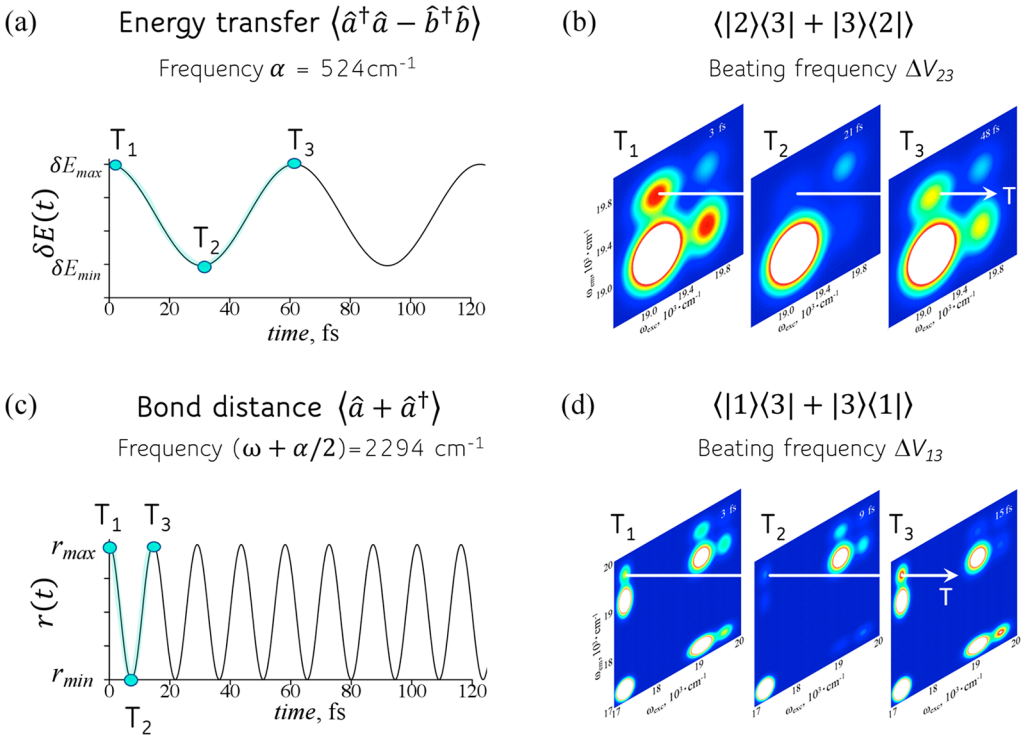

Figure 2. Emulation of vibrational dynamics. (a) Energy transfer $\delta E(t)$ from a hotter to a colder vibration, eq 3, and (c) bond displacement $r(t)$ vs time. (b, d) Evolution of the coherences in 2D frequency maps, computed for a 3% size dispersion, shown at different values of the delay time T between the first and second laser pulses as used in 2D electronic spectroscopy. These values of T are shown on the plots of the energy transfer and bond distance vs time. Different regions on the 2D map are used to compute the low-frequency oscillation of the energy transfer and high-frequency oscillations of the bond. See the SI, S3, for more details about computing such maps.

modes.[37] It is, however, physically rather different than the quantum device we use for the simulation, a device (i.e., hardware) that is built on the ultrafast dynamics of electronically excited states. In the main text, we discuss a device using just one semiconducting CdSe nanometric quantum dot with two electronically excited states, S_1 and S_2 (Scheme 1). At very high spectral resolution, each one of the two excited states is split by spin-orbit and crystal-field couplings[38−41] to 12 fine structure states, so $1(S_0) + 12(S_1) + 12(S_2) = 25$ states per dot (including the ground state) and there are $(25)^2$ operators that require high resolution to be observable. (Recall that expectation values for these operators are logic variables). This high resolution is not achievable with the currently available size dispersion of the dots. At an intermediate resolution that is already experimentally available,[25] each band of 12 states is resolvable into two bands of 4 and 8 states, respectively. See Figure 1 and Figures S2 and S3 in the SI. For specific QD sizes and limited size dispersion, the four bands do not overlap and each band can be separately optically addressed, so for intermediate resolution two bands for each excited state or $(1(S_0) + 2(S_1) + 2(S_2))^2 = 5^2$ logic variables are already experimentally available using only the two lowest electronically excited states of a single dot. At a higher size dispersion, one can have only three states or $(1(S_0) + 1(S_1) + 1(S_2))^2 = 9$ variables using a single dot.

For a quantum dot dimer, using the two lowest excited states on each monomer at the lowest resolution gives $(1(S_0) + 1(S_{1,A}) + 1(S_{2,A}) + 1(S_{1,B}) + 1(S_{2,B})) = 5$ states or 5^2 variables. Accounting for the fine structure splittings in the quantum dot dimer provides 48 states at the highest resolution, a resolution that will not be achievable due to the size dispersion of colloidal QD and the thermally induced transition between states. We emphasize the question of frequency resolution because the inevitable size dispersion of quantum dots means that the different spectroscopic transitions have a finite width due to the size variation.[42] Not all coherences can, in practice, be resolved. For example, we can emulate the dynamics of the two coupled harmonic oscillators, only for a limited number of vibrational periods, a time scale of about 200 fs, during which the set of operators that describe the electronic eigenstates of the computing device remains closed under commutation. At longer times, the coupling to the phonons and transfer of population between states due to the coupling to the environment leads to a loss of the closure property for the device.

The physical system we aim to simulate is the dynamics of two coupled oscillators. In the main text, we use the simplest but most realistic Hamiltonian, that of two coupled harmonic oscillators. This Hamiltonian can be written as

$$\hat{H} = \omega_a \hat{a}^\dagger \hat{a} + \omega_b \hat{b}^\dagger \hat{b} + (\hbar\alpha/2)(\hat{a}^\dagger \hat{b} + \hat{b}^\dagger \hat{a}) \quad (2)$$

where $\hat{a}$ and $\hat{b}$ are the annihilation operators for the two bonds and $\hat{X} \equiv \hat{a}^\dagger \hat{b} + \hat{b}^\dagger \hat{a}$ is the coupling between the two bonds as described in a force field model.[37] It is a harmonic coupling in that it describes only a one-quantum exchange between the two local bonds. In the SI, Section S1, we refine this description in two directions. One is that we allow a Fermi-type coupling which is relevant when the frequency of the faster mode is about twice the frequency of a slower mode. So one quantum of the fast mode is exchanged with two quanta of the slow one. This 1:2 frequency match is typical of the symmetric stretch and bending modes in linear triatomic

https://dx.doi.org/10.1021/acs.jpclett.0c01880
J. Phys. Chem. Lett. 2020, 11, 6990−6995

molecules (SI, Section S1.4). The other extension we discuss in the SI is when the two local modes are anharmonic Morse-type oscillators[43−45] (SI, Section S1.5).

In the main text, we first consider the case when the two local harmonic oscillators are identical, $\omega_a = \omega_b = \omega$ (e.g., CO_2), and there is an initial state that is not an equilibrium state but is stationary when there is no coupling, $\alpha = 0$. We compute a classical-like periodic quantity, the quantum mechanical energy transfer between the two oscillators. Then we discuss a state when initially the two bonds are displaced from their equilibrium distances. This more general case can also be simulated by a single quantum dot.

To compute the energy transfer, note that for the Hamiltonian (eq 2) the number of vibrational quanta $\hat{N} = \hat{a}^\dagger\hat{a} + \hat{b}^\dagger\hat{b}$ is a constant of the motion $[\hat{H}, \hat{N}] = 0$, while the difference $\hat{Z} = \hat{a}^\dagger\hat{a} - \hat{b}^\dagger\hat{b}$ is periodic in time $d\hat{Z}/dt = \alpha\hat{Y}$, $d\hat{Y}/dt = -\alpha\hat{Z}$, where $\hat{Y} = i(\hat{a}\hat{b}^\dagger - \hat{a}^\dagger\hat{b})$. It follows that $\hat{Z}(t) = \hat{Z}(0)\cos\alpha t$, and the energy transfer at time t is

$$\delta E = \omega(\langle\hat{Z}\rangle(t) - \langle\hat{Z}\rangle(0)) = \omega\langle\hat{Z}\rangle(0)(\cos(\alpha t) - 1) \tag{3}$$

where $\omega\langle\hat{Z}\rangle(0) = \omega\langle\hat{a}^\dagger\hat{a} - \hat{b}^\dagger\hat{b}\rangle(0)$ is the initial mismatch in energy of the two oscillators. See the SI, Section S1.1, for more details and Figure 2(a,b) for an example of a simulated energy transfer.

The energy transfer can be read from the time-dependent evolution of the mean values of the populations in the two lowest excited eigenstates 1 and 2 of a single dot and of the coherence between these two states, after a sequence of fs laser pulses that builds the electronic coherence between them:

$$\langle 1|\hat{\rho}(t)|2\rangle + \langle 2|\hat{\rho}(t)|1\rangle = 2\sqrt{\langle 1|\hat{\rho}(t)|1\rangle\langle 2|\hat{\rho}(t)|2\rangle}\,\cos(\Delta E t/\hbar) \tag{4}$$

The density matrix of the device at time t is $\hat{\rho}(t)$, $\hat{\rho}(t) = \sum_{i,j}^{N} x_{ij}(t)\hat{X}_{ij}$, and ΔE is the energy spacing between the two excited states. It is read by the oscillation of the coherence, which is the mean value of the projection operator $\hat{X}_{12} = |1\rangle\langle 2|$. The amplitude is read by the amplitude of the oscillation of the coherence, Figure 2(b,d), or from the population of the two states, entries that appear along the diagonal in a coherence map representation of the output of 2D electronic spectroscopy.[31,32]

To describe the energy of each local oscillator, their coupling, and the resulting energy transfer, we need the closed algebra of five operators, $\hat{I}$, $\hat{N}$, $\hat{Z}$, $\hat{X}$, $\hat{Y}$ where $(\hat{N} \pm \hat{Z})$ specifies the number of quanta in each oscillator. To compute the expectation values of quantum mechanical operators such as $\langle a\rangle$ or $\langle b^\dagger\rangle$, we need to enlarge the algebra. It turns out that adding the four operators a, $a^\dagger$, b, and $b^\dagger$ to the previous five provides a nine (Lie)-operator algebra that is closed under commutation with the Hamiltonian (eq 5). The algebra is also closed for inequivalent local modes and even for a more general Hamiltonian as shown in the SI (Section S1.3). Nine operators is the number of operators corresponding to the three lowest electronic states of a single QD. The full details are given in the SI (Section S1.2), and here we discuss the case of equivalent oscillators, when the two operators $\hat{a}$ and $\hat{b}$ and separately $\hat{a}^\dagger$ and $\hat{b}^\dagger$ form two closed subalgebra sets. For example, for the first pair,

$$\frac{d}{dt}\begin{pmatrix}\hat{a}\\ \hat{b}\end{pmatrix} = -i\begin{pmatrix}\omega & \alpha/2\\ \alpha/2 & \omega\end{pmatrix}\begin{pmatrix}\hat{a}\\ \hat{b}\end{pmatrix} \tag{5}$$

with two eigenfrequencies $(\omega + \alpha/2)$ and $(\omega - \alpha/2)$ and eigenvectors $\hat{a} \pm \hat{b}$ and similarly for the second pair. For two identical local oscillators that are initially at rest and equally displaced from their equilibrium length, $\langle\hat{a}(t)\rangle = \langle\hat{a}(0)\rangle \exp(-i(\omega + \alpha/2)t)$ and similarly for its complex conjugate $\langle\hat{a}^\dagger(t)\rangle$. The bond length oscillates as $\langle r(t)\rangle = \langle r(0)\rangle \cos((\omega + \alpha/2)t)$ while the initial mean momentum is zero and oscillates as $\sin((\omega + \alpha/2)t)$. See the details of the analytical solution in the SI, Section S1.2.

To simulate the dynamics of the nine operators, we need to compute three variables that oscillate with time at different frequencies. An example of the oscillation of the bond is shown in Figure 2(c,d). These oscillations are resolvable even for the larger dispersion of the sizes of the QD (Figure S5 in the SI). Variables changing with a low frequency, such as energy transfer, 524 cm^{-1}, are read closer to the diagonal, so the broadening due to size dispersion is more critical (Figure S6 of the SI).

An example of two coupled shifted oscillators using nine-membered closed algebra is discussed in the SI, Section S1.3. Finally, we comment that one can have quite realistic physical situations where one is unable to close algebra of a few operators. At the same time, it follows from the discussion in connection with eq 1 that in an isolated quantum mechanical system of N states there is always (nonunique) closed algebra of N^2 operators. Coherences $\hat{X}_{ij} \equiv |i\rangle\langle j|$, $i, j = 1, 2,.., N$ are a convenient set of such operators. When quantum states $|i\rangle$ and $|j\rangle$ are connected by a transition dipole, such coherences can be detected by optical means. For electronic states, this could be pump−probe transient absorption spectroscopy or a nonlinear method such as 2D electronic spectroscopy or four-wave mixing.

In this letter, we used only the time dependence of the coherences of the quantum device to simulate the physical system. This is less of a restriction than one might think. To see the point, consider the equations of motion of the observables of the physical system. Arrange the observables as components of a vector. The rate of change of this vector is described by a Liouvillian matrix (e.g., eq S27 in the SI). When we diagonalize this Liouvillian matrix, we get a set of eigenfrequencies that fully characterize the time evolution of the physical variables. We simulate the time dependence by the oscillation of the coherences of the quantum device, and size dispersion is beneficial for the fine-tuning of the oscillation frequencies.

■ ASSOCIATED CONTENT

Supporting Information

The Supporting Information is available free of charge at https://pubs.acs.org/doi/10.1021/acs.jpclett.0c01880.

Details on the closed algebra for two inequivalent harmonic oscillators, Fermi-type anharmonic coupling, coupling of anharmonic oscillators, spin−orbit coupling of a single dot, and modeling of the 2D electronic spectroscopy maps (PDF)

https://dx.doi.org/10.1021/acs.jpclett.0c01880
J. Phys. Chem. Lett. 2020, 11, 6990−6995

AUTHOR INFORMATION

Corresponding Author

F. Remacle − *Theoretical Physical Chemistry, UR MolSys B6c, University of Liège, B4000 Liège, Belgium; The Fritz Haber Center for Molecular Dynamics and Institute of Chemistry, The Hebrew University of Jerusalem, Jerusalem 91904, Israel;* orcid.org/0000-0001-7434-5245; Email: fremacle@uliege.be

Authors

Ksenia Komarova − *The Fritz Haber Center for Molecular Dynamics and Institute of Chemistry, The Hebrew University of Jerusalem, Jerusalem 91904, Israel;* orcid.org/0000-0001-6603-1377

Hugo Gattuso − *Theoretical Physical Chemistry, UR MolSys B6c, University of Liège, B4000 Liège, Belgium*

R. D. Levine − *The Fritz Haber Center for Molecular Dynamics and Institute of Chemistry, The Hebrew University of Jerusalem, Jerusalem 91904, Israel; Department of Chemistry and Biochemistry and Department of Molecular and Medical Pharmacology, David Geffen School of Medicine, University of California, Los Angeles, California 90095, United States*

Complete contact information is available at: https://pubs.acs.org/10.1021/acs.jpclett.0c01880

Notes

The authors declare no competing financial interest.

ACKNOWLEDGMENTS

We thank Prof. Elisabetta Collini for many incisive discussions about the experiments on the device. This work was supported by FET open EC project COPAC no. 766563 and the Fonds National de la Recherche Scientifique (F.R.S-FNRS, Belgium), nos. T.0205.20 and J.0012.18. Computational resources have been provided by the COPAC project and by the Consortium des Equipements de Calcul Intensif (CECI), funded by the F.R.S.-FNRS under grant no. 2.5020.11.

REFERENCES

(1) Feynman, R. P. Simulating physics with computers. *Int. J. Theor. Phys.* **1982**, *21*, 467−488.

(2) Milburn, G. J. *The Feynman Processor: Quantum Entanglement and the Computing Revolution*; Perseus Books: Reading, MA, 1999.

(3) Nielsen, M. A.; Chuang, I. L. *Quantum Computation and Quantum Information*; Cambridge University Press: Cambridge, 2010.

(4) Shapiro, M.; Brumer, P. *Quantum Control of Molecular Processes*; Wiley: Weinheim, 2012.

(5) Yuen-Zhou, J.; Krich, J. J.; Kassal, I.; Johnson, A. S.; Aspuru-Guzik, A. Ultrafast Spectroscopy. In *Quantum Information and Wavepackets*; IOP Publishing: Bristol, 2014. DOI: 10.1088/978-0-750-31062-8.

(6) Kais, S. *Quantum Information and Computation for Chemistry*; Wiley and Sons: Hoboken, NJ, 2014; Vol. *154*.

(7) Lee, J.; Huggins, W. J.; Head-Gordon, M.; Whaley, K. B. Generalized Unitary Coupled Cluster Wave functions for Quantum Computation. *J. Chem. Theory Comput.* **2019**, *15*, 311−324.

(8) Albash, T.; Lidar, D. A. Adiabatic quantum computation. *Rev. Mod. Phys.* **2018**, *90*, 015002.

(9) Gyongyosi, L.; Imre, S. A Survey on quantum computing technology. *Comput. Sci. Rev.* **2019**, *31*, 51−71.

(10) National Academies of Sciences Engineering and Medicine; *Quantum Computing: Progress and Prospects (2019)*; The National Academies Press: Washington, DC, 2019.

(11) Arute, F.; et al. Quantum supremacy using a programmable superconducting processor. *Nature* **2019**, *574*, 505−510.

(12) Smith, A.; Kim, M. S.; Pollmann, F.; Knolle, J. Simulating quantum many-body dynamics on a current digital quantum computer. *npj Quantum Inf* **2019**, *5*, 106.

(13) Cao, Y.; et al. Quantum Chemistry in the Age of Quantum Computing. *Chem. Rev.* **2019**, *119*, 10856−10915.

(14) Xia, R.; Kais, S. Quantum machine learning for electronic structure calculations. *Nat. Commun.* **2018**, *9*, 4195.

(15) Argüello-Luengo, J.; González-Tudela, A.; Shi, T.; Zoller, P.; Cirac, J. I. Analogue quantum chemistry simulation. *Nature* **2019**, *574*, 215−218.

(16) Hempel, C.; et al. Quantum Chemistry Calculations on a Trapped-Ion Quantum Simulator. *Phys. Rev. X* **2018**, *8*, 031022.

(17) Yung, M. H.; Casanova, J.; Mezzacapo, A.; McClean, J.; Lamata, L.; Aspuru-Guzik, A.; Solano, E. From transistor to trapped-ion computers for quantum chemistry. *Sci. Rep.* **2015**, *4*, 3589.

(18) Daskin, A.; Kais, S. Direct application of the phase estimation algorithm to find the eigenvalues of the Hamiltonians. *Chem. Phys.* **2018**, *514*, 87−94.

(19) Ciliberto, C.; Herbster, M.; Ialongo Alessandro, D.; Pontil, M.; Rocchetto, A.; Severini, S.; Wossnig, L. Quantum machine learning: a classical perspective. *Proc. R. Soc. London, Ser. A* **2018**, *474*, 20170551.

(20) Rebentrost, P.; Steffens, A.; Marvian, I.; Lloyd, S. Quantum singular-value decomposition of nonsparse low-rank matrices. *Phys. Rev. A: At., Mol., Opt. Phys.* **2018**, *97*, 012327.

(21) Schuld, M.; Sinayskiy, I.; Petruccione, F. Prediction by linear regression on a quantum computer. *Phys. Rev. A: At., Mol., Opt. Phys.* **2016**, *94*, 022342.

(22) Gao, X.; Zhang, Z. Y.; Duan, L. M. A quantum machine learning algorithm based on generative models. *Sci. Adv.* **2018**, *4*, No. eaat9004.

(23) *Hearing-the-Quantum Top 10 Quantum Experiments in 2019*, accessed https://medium.com/swlh/top-quantum-computing-experiments-of-2019-1157db177611.

(24) Pednault, E.; Gunnels, J.; Maslov, D.; Gambetta, J. *On Quantum Supremacy*, accessed https://www.ibm.com/blogs/research/2019/10/on-quantum-supremacy/.

(25) Collini, E.; Gattuso, H.; Bolzonello, L.; Casotto, A.; Volpato, A.; Dibenedetto, C. N.; Fanizza, E.; Striccoli, M.; Remacle, F. Quantum Phenomena in Nanomaterials: Coherent Superpositions of Fine Structure States in CdSe Nanocrystals at Room Temperature. *J. Phys. Chem. C* **2019**, *123*, 31286−31293.

(26) Collini, E.; et al. Room-Temperature Inter-Dot Coherent Dynamics in Multilayer Quantum Dot Materials. *J. Phys. Chem. C* **2020**, *124*, 16222.

(27) Kambhampati, P. Unraveling the Structure and Dynamics of Excitons in Semiconductor Quantum Dots. *Acc. Chem. Res.* **2011**, *44*, 1−13.

(28) Caram, J. R.; Zheng, H.; Dahlberg, P. D.; Rolczynski, B. S.; Griffin, G. B.; Dolzhnikov, D. S.; Talapin, D. V.; Engel, G. S. Exploring size and state dynamics in CdSe quantum dots using two-dimensional electronic spectroscopy. *J. Chem. Phys.* **2014**, *140*, 084701.

(29) Turner, D. B.; Hassan, Y.; Scholes, G. D. Exciton Superposition States in CdSe Nanocrystals Measured Using Broadband Two-Dimensional Electronic Spectroscopy. *Nano Lett.* **2012**, *12*, 880−886.

(30) Cassette, E.; Dean, J. C.; Scholes, G. D. Two-Dimensional Visible Spectroscopy For Studying Colloidal Semiconductor Nanocrystals. *Small* **2016**, *12*, 2234−2244.

(31) Cho, M. *Two-Dimensional Optical Spectroscopy*; CRC Press: Boca Raton, FL, 2009.

(32) Mukamel, S. *Principle of Nonlinear Optical Spectroscopy*; Oxfrod University Press: Oxford, 1995.

(33) Warren, W. S. The Usefulness of NMR Quantum Computing. *Science* **1997**, *277*, 1688.

(34) Gattuso, H.; Levine, R. D.; Remacle, F., Massively Parallel Classical Logic via Coherent Dynamics of an Ensemble of Quantum Systems with Dispersion in Size. *Proc. Natl. Acad. Sci. U.S.A.* **2020**, accepted. DOI: 10.26434/chemrxiv.12370538.v1.

(35) Alhassid, Y.; Levine, R. D. Connection between the maximal entropy and the scattering theoretic analyses of collision processes. *Phys. Rev. A: At., Mol., Opt. Phys.* **1978**, *18*, 89−116.
(36) Gilmore, R. *Lie Groups, Lie Algebras and Some of Their Applications*; Dover: Mineola, 2012.
(37) Herzberg, G. *Molecular Spectra and Molecular Structure*; Van Nostrand: New York, 1945; Vol. *II*.
(38) Efros, A. L.; Rosen, M. The electronic structure of semiconducting nanocrystal. *Annu. Rev. Mater. Sci.* **2000**, *30*, 475−521.
(39) Sercel, P. C.; Efros, A. L. Band-Edge Exciton in CdSe and Other II−VI and III−V Compound Semiconductor Nanocrystals − Revisited. *Nano Lett.* **2018**, *18*, 4061−4068.
(40) Norris, D. J.; Bawendi, M. G. Measurement and assignment of the size-dependent optical spectrum in CdSe quantum dots. *Phys. Rev. B: Condens. Matter Mater. Phys.* **1996**, *53*, 16338−16346.
(41) Wong, C. Y.; Scholes, G. D. Using two-dimensional photon echo spectroscopy to probe the fine structure of the ground state biexciton of CdSe nanocrystals. *J. Lumin.* **2011**, *131*, 366−374.
(42) Gattuso, H.; Fresch, B.; Levine, R. D.; Remacle, F. Coherent Exciton Dynamics in Ensembles of Size-Dispersed CdSe Quantum Dot Dimers Probed via Ultrafast Spectroscopy: A Quantum Computational Study. *Appl. Sci.* **2020**, *10*, 1328.
(43) Child, M. S.; Lawton, R. T. Local and normal vibrational states: a harmonically coupled anharmonic-oscillator model. *Faraday Discuss. Chem. Soc.* **1981**, *71*, 273−285.
(44) Lehmann, K. K. On the relation of Child and Lawton's harmonically coupled anharmonic−oscillator model and Darling−Dennison couplinga). *J. Chem. Phys.* **1983**, *79*, 1098.
(45) Levine, R. D. Representation of one-dimensional motion in a morse potential by a quadratic hamiltonian. *Chem. Phys. Lett.* **1983**, *95*, 87−90.

https://dx.doi.org/10.1021/acs.jpclett.0c01880
J. Phys. Chem. Lett. 2020, 11, 6990−6995